Available online at www.sciencedirect.com
ScienceDirect
Polymer 49 (2008) 843–856
polymer
www.elsevier.com/locate/polymer

Well-defined core-shell structures based on silsesquioxane microgels: Grafting of polystyrene via ATRP and product characterization

Leszek Jakuczek [a,b,*], Jochen S. Gutmann [b,c,**], Beate Müller [b], Christine Rosenauer [b], Danuta Żuchowska [a]

[a] *Wroclaw University of Technology, Faculty of Chemistry, Department of Polymer Engineering and Technology, Wybrzeze Wyspianskiego 27, 50-370 Wroclaw, Poland*
[b] *Max Planck Institute for Polymer Research, Ackermannweg 10, 55128 Mainz, Germany*
[c] *Johannes Gutenberg University, Institute for Physical Chemistry, Welderweg 11, 55099 Mainz, Germany*

Received 7 May 2007; received in revised form 26 November 2007; accepted 18 December 2007
Available online 31 December 2007

Abstract

Silsesquioxane microgel nanoparticles characterized by low diameters (below 30 nm) and reduced polydispersity can be produced in an acid-catalyzed sol–gel process in an aqueous microemulsion. Suitable surface modification of such structures leads to macroinitiators for atom-transfer radical polymerization (ATRP). This polymerization method was applied in order to graft polystyrene chains onto the surface of the microgels. Well-defined structures exhibiting a core-shell architecture were produced with the M_w of grafted polymers ranging from 8.5 to about 30 kg/mol. The products were extensively characterized with light scattering, X-ray scattering, thermal analysis (TGA/DSC) and microscopy (TEM/SEM) to obtain information on parameters characterizing polystyrene brush. Polymer-grafted nanoparticles will be used for the modification of homopolymer and block copolymer matrices.
© 2007 Published by Elsevier Ltd.

Keywords: Core-shell structures; Silsesquioxane microgel nanoparticles; Polymer brush

1. Introduction

Polymer-based nanocomposites have been an object of intensive research since almost 15 years. Several factors, like low filler loading (compared to ''classic'', μm-sized reinforcing agents) combined with impressive enhancement ability decided about the growing interest on this class of materials. The scope of their utilization has been significantly broadened over years – starting from ''simple'' improvement of mechanical or thermal properties (e.g. polymer–clay nanocomposites [1,2]) up to such advanced areas like optoelectronics [3–5] and energy conversion [6,7].

In almost all cases an inherent incompatibility between inorganic fillers and organic polymer matrix is a central difficulty in composite preparation. In order to overcome this problem several approaches – like surfactant absorption [8], ion exchange [1,2,9] and polymer grafting [10] were developed. All those approaches focus almost exclusively at the modification of the filler surface. Especially in the case of polymer grafting, the requirement of a high compatibility between matrix and reinforcing agent is often envisioned to be facilely realized.

However, both theoretical [11–14] and experimental results [10,15–17], obtained for the fillers with surface-grafted polymer brushes, alluded to some additional factors that must be taken into consideration – e.g. the molecular weight and grafting density of immobilized chains. In a limiting case grafted filler cannot be uniformly dispersed in the matrix and

* Corresponding author. Wroclaw University of Technology, Chemical Faculty, Department of Polymer Engineering and Technology, Wybrzeze Wyspianskiego 27, 50-370 Wroclaw, Poland.
** Corresponding author. Max Planck Institute for Polymer Research, Ackermannweg 10, 55128 Mainz, Germany.
E-mail addresses: leszek.jakuczek@pwr.wroc.pl (L. Jakuczek), gutmann@mpip-mainz.mpg.de (J.S. Gutmann).

0032-3861/$ - see front matter © 2007 Published by Elsevier Ltd.
doi:10.1016/j.polymer.2007.12.030

phase separation occurs – as stated by a few research teams [10,15–17].

The immobilization of polymer chains onto the substrate can be realized via several methods. Physical adsorption or chemical reaction of previously prepared macromolecules constitute so-called ''grafting to'' approaches, which allow to preserve an excellent control over chain properties (especially, concerning molecular weight and polydispersity). However, the accessibility of reactive surface groups is severely hindered after attachment of a few macromolecules, implying unsatisfactory grafting densities. The removal of significant amount of ungrafted polymer requires tedious procedures, especially in case of systems consisting of polymer and colloid particles [10].

The second possibility is offered by the ''grafting from'' approaches based on surface-initiated growth of polymer chains. In this context, controlled free-radical polymerization techniques – e.g. atom-transfer-radical-polymerization (ATRP) have gained a lot of interest. These methods appear to offer the best way for the preparation of hybrid organic–inorganic materials. Devoid from the high sensitivity towards impurities characterizing ionic polymerization processes, they allow to synthesize well-defined structures with grafted polymer chains [18–20]. High grafting densities, good control over the reaction course and ease of copolymerization are the most important advantages of this approach. On the other hand, some monomers (e.g. dienes) cannot be still polymerized according to this route [21]. The development of new catalytic systems and preparative routes would be required to overcome this limitation.

The main scope of our work is related to investigation of interactions between polymer matrix and polymer-grafted (''hairy'') filler. We decided to choose polystyrene (PS) homopolymer matrix and silsesquioxane nanoparticles grafted with PS in an ATRP process, because this enabled us to use very well-defined components. Various analytical techniques – like electron microscopy, static and dynamic light scattering (SLS and DLS), small-angle X-ray scattering (SAXS), gel-permeation chromatography (GPC) and thermogravimetry (TGA) – were used to fully characterize the investigated systems and to define the conditions for homogeneous filler dispersion.

The results presented here were thought to be a preceding step in our investigation on the influence of such organic–inorganic core-shell structures on the block copolymer matrices.

2. Experimental part

2.1. Materials and syntheses

2.1.1. Synthesis of the silane ATRP initiator

We followed the preparation route of the ATRP initiator described by Ramakrishnan et al. [22]. 2-Bromoisobutyrate bromide (98%, Aldrich) was added dropwise to the solution of allyl alcohol (99%, Aldrich) and freshly distilled trimethylamine (Aldrich) in dichloromethane (HPLC-grade, Fisher). The reactor was placed in an ice bath in order to prevent an uncontrolled reaction.

After about 16 h the mixture was diluted with diethyl ether (p.a. – grade, Riedel de Haën) and the precipitated salt was separated by filtration. The mixture of liquid products was repeatedly washed with: 1% hydrochloric acid (p.a., Fluka), 5% sodium bicarbonate (p.a., Fisher) solutions and, finally, with distilled water. After drying over $MgSO_4$ (WTL Laborbedarf) and two-stage distillation the main product – allyl 2-bromoisobutyrate – was recovered.

Allyl ester and distilled dimethylchlorosilane (98%, Fluka) or dimethylethoxysilane (97%, ABCR) were then coupled via hydrosillylation process. The reaction was catalyzed with platinum on activated charcoal (10% Pt, Fluka). The colourless, oily products – denoted by ATRP–Cl and ATRP–Et (attached structures – Fig. 1), respectively – were purified by two-stage distillation and stored in desiccator under inert atmosphere (argon, Ar).

2.1.2. Microgel synthesis

The synthesis of silsesquioxane microgel (μgel) nanoparticles in microemulsion was firstly introduced by Baumann and further developed by Schmidt and coworkers [23–28]. One of its variants – with dodecylbenzenesulfonic acid (DBA) as a surfactant – was originally introduced by Lindenblatt et al. [10]. The synthesis described below is a modification of this method. The reactions (with corresponding abbreviations used in text) are depicted in the attached scheme (Fig. 2). The intermediate product – non-modified μgel (denoted with an asterisk) cannot be separated without further treatment and must be stabilized against agglomeration.

Distilled methyltrimethoxysilane (M_3MeS 99%, Aldrich) was added dropwise to vigorously stirred aqueous solution of DBA (97%, Aldrich). We decided to follow the acid-catalyzed approach by Lindenblatt due to the better microemulsion stability and reaction yield observed in this case (as compared to the basic system based on the benzethonium chloride).

The nanoparticles were basically formed after about 6 h. In order to suppress agglomeration processes, the obtained microgel particles had to be modified. Modification was initially carried out in aqueous phase with trimethylethoxysilane (3MEtS; 98% Wacker, Aldrich) and excess ATRP–Et. After about 24 h the microgel particles were precipitated with

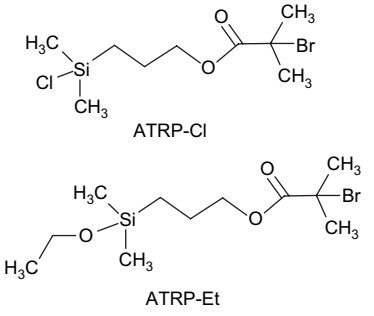

Fig. 1. Chemical structures of the silane modifying agents used as ATRP initiators.

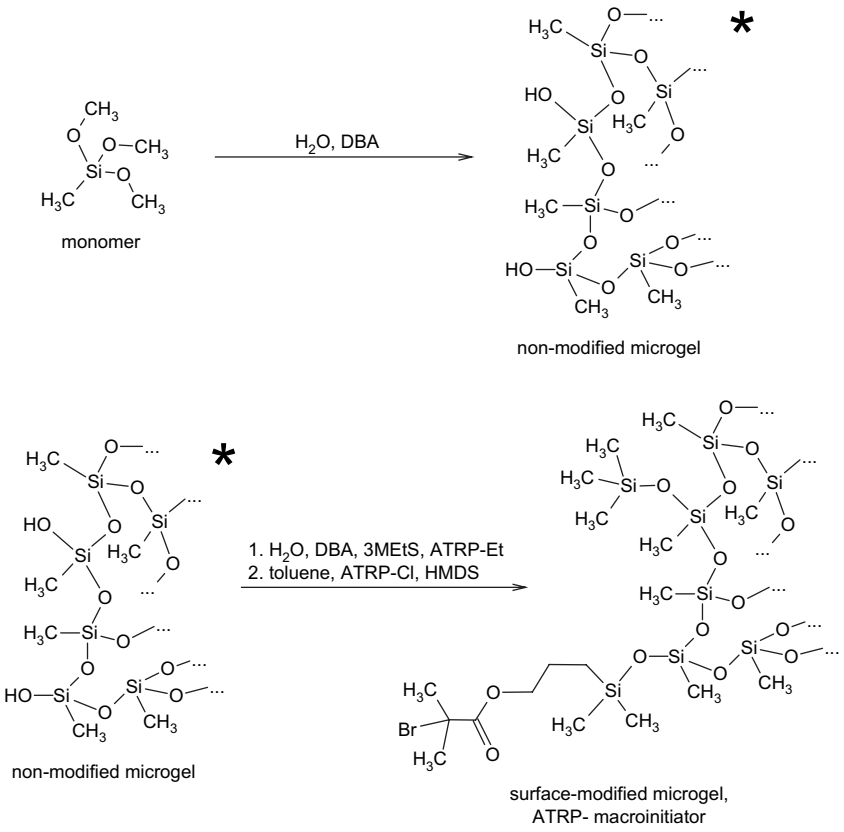

Fig. 2. Schematic representation for the synthesis of the silsesquioxane microgel nanoparticles functionalized with the ATRP-initiators.

methanol (MeOH, HPLC-grade, Fisher). The precipitate was separated by filtration and washed with MeOH to remove surfactant. Wet product was then re-dispersed in toluene (p.a. – grade, Riedel de Haën) and residual water and MeOH were removed under reduced pressure. After additional drying over $MgSO_4$, the modification with ATRP–Cl was continued, followed by the subsequent addition of 1,1,1,3,3,3-hexamethyldisilazane (HMDS, 97%, Janssen) to ensure the complete removal of silanol groups (according to the procedure described in Ref. [18]). Afterwards, the main product was recovered by precipitation, filtered and repeatedly washed with MeOH. The microgel macroinitiators were then dried under reduced pressure and stored in the fridge.

The amount of particular reagents (monomer, ATRP initiators, HMDS, 3MEtS) was varied in order to find out, whether it is possible to tailor the surface coverage (for detailed information – see Table 1) and subsequent comments in Section 3. The concentration of the ATRP–Et used in the first stage of reaction was changed between 6.5 and 10% of the monomer amount. For the second stage of the process (after transfer to toluene) the amount of the ATRP initiators was set to be about 20, 25 and 30 mol.% of the monomer amount.

2.1.3. ATRP polymerization

Styrene (99%, Acros Organics) was filtered through alumina (Fluka) to remove stabilizers, subsequently distilled under reduced pressure, and stored under air at −20 °C. Copper(I) bromide (98%, Aldrich), was purified prior to use, according to the method described in Bumbu et al. [29]. Copper(II) bromide (99.999%, Aldrich) was used as supplied. The *N*,*N*′,*N*′,*N*″,*N*″-pentamethyldiethylenetriamine (PMDTA; 99%, Aldrich) was vacuum distilled and stored under argon in the fridge. The solvent (toluene) and precipitant (MeOH) were used as received.

All liquid components (monomer, solvent and amine) were extensively bubbled with Ar to remove residual oxygen prior to use.

Typically, about 1 g of Br-functionalized microgels (about 0.43–0.50 mmol Br/g, depending on the microgel type), 0.114 g (0.8 mmol) of CuBr and 0.134 g (0.6 mmol) $CuBr_2$ were degassed under vacuum for 3 h in a 100 ml Schlenk-flask. Toluene (15–20 ml) was added under Ar purge,

Table 1
Amounts of monomer and silane ATRP-initiators used in particular syntheses

Microgel	Monomer amount [mmol]	Total amount [mmol/% of the monomer amount] of the ATRP initiators (ATRP–Et or ATRP–Cl) added at	
		First stage of reaction (aqueous dispersion)	Second stage of reaction (organic dispersion)
MG11	147.2	14.8/10.06	44.2/30.02
MG12	264.4	26.2/9.92	65.1/24.62
MG13	268.3	17.6/6.56	80.1/29.84
MG14	300.8	20.2/6.70	75.3/25.05
MG15	235.9	15.3/6.50	58.5/24.8
MG17	133.8	8.8/6.55	27.1/20.25

followed by the dispergation of solid components (ultrasonic bath, 30 min). Afterwards, usually about 20 g (192 mmol) of styrene and 0.254 g (1.47 mmol) of PMDTA were introduced using a syringe, under Ar flow. We commonly kept the solvent volume ratio at about 50% and used a 5% excess of amine (for better catalyst dispersion). Afterwards the dark green mixture was immediately subjected to three freeze-pump-thaw cycles. The exact dispergation of the copper salts was carried out in an ultrasonic bath after the first cycle.

The mixture was allowed to polymerize at 90 °C for several hours. The average monomer conversion was kept below 20%. Upon reaching the desired conversion, the reaction was interrupted and the mixture was diluted with THF (p.a. – grade, Acros) and consequently stirred for 1 h with ion-exchange resin (Dowex® Marathon® Msc, Aldrich) to remove residual copper. The resin was separated by filtration and the core-shell structures (polystyrene-grafted microgel, further denoted as: PS-*g*-μgels) were recovered by precipitation into MeOH. Finally, the white, fluffy product was dried for 24 h at 80 °C under reduced pressure.

2.1.4. Cleaving of the grafted polystyrene chains

The grafted polymer was cleaved according to the procedure described elsewhere [18–20]. In order to remove the silsesquioxane network about 0.1–0.15 g of PS-*g*-μgels were dispersed in 10 ml of toluene together with 0.2 g of the phase-transfer catalyst – trioctylmethylammonium chloride (Adogen® 464, Acros). Finally about 1.5 g of 49% HF (Fluka) was added and the mixture was allowed to react for 24 h under intensive stirring. The polymer was recovered then by precipitation into MeOH and subsequent filtration. After vacuum drying molecular weight and polydispersity of the grafted chains were analyzed with the GPC.

2.2. Characterization methods and sample preparation

Solution ^{1}H NMR spectra of the synthesized compounds were recorded with the Bruker Avance spectrometer operating at 250 MHz. The substances were dispersed in appropriate deuterated solvents ($CDCl_3$, d_8-toluene or *d*-THF) prior to analysis. Solid-state CP (cross-polarization) MAS (magic-angle-spinning) ^{29}Si NMR measurements of the microgels were carried out on a 600 MHz Bruker Avance spectrometer.

All scanning images were recorded using the LEO Gemini 1530 microscope operating at low accelerating voltage (1.0 to max. 3 kV). Samples of neat μ-gels and nanoparticles with grafted PS (PS-*g*-μgels) were prepared by re-dispersing the mentioned substances in toluene (to avoid the presence of agglomerates dispersions were additionally sonicated for 1 h) and subsequent spin-coating on the silicon substrate at about 2000 rpm.

Transmission electron microscopy (TEM) images were recorded on a Tecnai FEI F20 microscope. All samples of nanoparticles were prepared by depositing a droplet of highly diluted microgel dispersions in toluene (mass concentration below 0.01%) onto the carbon substrate. The solvent was allowed to evaporate afterwards. Subsequently micrographs were recorded and diameters as well as values of standard deviation were calculated for several hundreds of particles.

GPC – analyses of molecular weight and polydispersity of polymers and microgels were conducted using the four-component system Water Alliance 2000, consisting of the Waters 590 pump and three columns (pore sizes: 10^6, 10, 500 Å).

The refractive index increment d*n*/d*c* – necessary for evaluation of the grafted PS amount – was investigated using the scanning Michelson interferometer. As a source an Ar-Ion laser (Siemens) with 25 mW output power, operating at 633 nm was used. All measurements were conducted at 25 °C.

Dynamic and static light scattering (DLS/SLS) experiments were performed at 25 °C, using a setup consisting of an ALV 5000 digital correlator (320 channels), ALV-SP81 goniometer, an Avalanche Photodiode and an air-cooled He/Ne-laser operating at 632.8 nm and giving 20 mW output power. The intensity of scattered light was measured between 25 and 150° at a usual time resolution ranging from 10^{-3} to 10^{3} s. Light was polarized vertically with respect to the scattering plane using the Glan–Thomson polarizers with an extinction coefficient lower than 10^{-7}. When the recorded intensity was too high a reducing filter was used to attenuate the scattered light. The dimensions and molecular weight of the microgel nanoparticles were computed with ALV 5000 software (utilizing an approach based on Contin algorithm). The samples of the non-modified and PS-grafted microgels for DLS analyses were prepared by re-dispergation of the substances in toluene, yielding dilute dispersions (0.025 wt.% on average).

SAXS diffraction patterns of neat microgels were recorded in transmission mode using SAXS-setup consisting of MicroMaxx 007 rotating anode and 2D-Histar detector with a distance to sample of 1.78 m and angular resolution 0.01°. Scattering profiles were calculated for 2θ values between 0.20 and 1.90°, diffractograms were corrected for detector efficiency and distortion using GADDS software (Bruker).

Thermogravimetric analyses of the neat and polymer-grafted microgels were recorded using Mettler TGA-851 thermobalance (temperature interval: 25–700 °C, heating rate: 10 K/min, under air flow). Differential scanning calorimetry (DSC) experiments with PS-*g*-μgels were performed on a Mettler DSC 822 calorimeter within temperature interval 25–180 °C, at heating rate 10 K/min. All samples were subjected to the same temperature program with heating–cooling–heating cycles. First heating cycle allowed to erase the thermal history of the sample.

3. Results and discussion

3.1. Microgel synthesis

Silsesquioxane-based materials are characterized by the general formula $RSiO_{3/2}$, where R denotes the organic substituent (alkyl, aryl). Since the advent of nanotechnology they have been subject of intensive research mainly due to numerous possibilities of synthesis and modification of silsesquioxane-based nanostructures. Much interest was devoted to the preparation and property evaluation of so-called polyhedral

oligo-silsesquioxanes constituting the smallest organically-modified analogues of silica [30–33]. These nanostructures exhibit regular internal structure, but can exist in a variety of forms (e.g. cage- or ladder-like). Undoubtedly the most popular ones are the cubic oligo-silsesquioxanes (denoted with T_8) obtained by condesation of 8 monomer units and bearing 8 organic groups situated at the corners. The other available variants are T_4, T_{12} or T_{14} structures composed of 4, 12 and 14 monomeric units, respectively. Due to extremely high surface-to-volume ratio (particle dimension 0.5–0.7 nm [32]) these particles can be used e.g. as highly active fillers for polymer modification [31]. However, they are not the subject of our report and will therefore not be treated in much detail.

The family of silsesquioxane materials includes the amorphous products of organotrialkoxysilane polycondensation, either. These organosilicon microgels [23] or (polysilsesquioxane colloids [32]) of intermediate dimensions (from about five to several tens of nanometers) can be facilely produced in dispersed systems (emulsion or microemulsion) [23,24,34] and were a filler of choice in our case. We decided to make use of the synthetic method of sol–gel reaction in microemulsion introduced by Lindenblatt et al. [10]. It was based on techniques originally developed for the coating industry in the 60's and adapted later by Baumann and coworkers [23,24]. This preparative route has some important advantages, especially when referred to the Stöber's approach. The satisfactory dimensional control (shape regularity) during the nanoparticle synthesis in alcoholic solutions cannot be preserved below certain limiting value of product diameter (~35–40 nm) under standard conditions. However, such particles are still too big with respect to the domain size of commonly used block copolymers. The attempts to reduce the size of the colloids usually result in its higher polydispersity and perturbed form. Additionally, the mass fraction of the product (defined by the monomer amount) must also be limited, otherwise particle polydispersity will increase [35]. In comparison, the nanoparticles produced in the surfactant-supported systems (synthesis in reversed microemulsion reported by Arrigada and Osseo-Asare [36] and Chang and Fogler [37]) or according to so-called "seeding" technique (presented by Buining et al. [38]) exhibit more advantageous properties being characterized by smaller diameters, low polydispersity and regular shape. However, tedious purification and unsatisfactory yield of the product constitute the essential drawbacks of the method.

In contrast, the method of Baumann et al. and Lindenblatt et al. allows – due to the presence of the surfactant – to efficiently produce nanoparticles with diameters below 30 nm and preserved shape control. Upon changing the reaction conditions (e.g. monomer type, dosing sequence, type of modifying agent) diversified products exhibiting interesting physical properties – like amphiphilic character, adjustable degree of swelling, core-shell morphology – can be prepared [23–28]. The amphiphilic core-shell nanostructures can be obtained within a "one-pot" process using monomer mixtures and exhibit different character of the constituting parts (hydrophobic or hydrophilic) followed by different mechanical behavior. In these way the interactions between the chosen part of the structure (core, shell) and surrounding medium can be controlled (valuable feature with respect to sensors or medical applications [23–25]). Furthermore, hollow spheres (ideal drug carriers for certain applications) of controlled architecture can be synthesized by simply changing the ratio between di- and trialkoxysilanes [25]. The microgel synthesis offers also the possibility of obtaining well-defined nanostructures of regular shape and dimensions for further modification, like polymer grafting, dye-labelling [27]. Upon using different monomers, porosity of the microgel, its swelling behavior and the accessibility of the active groups under different conditions can be finely tuned.

Another important advantage of the chosen synthetic approach (especially, when compared to the W/O-microemulsions [36]) is the relatively low surfactant content (typically 0.8–1.4 wt.%) implying its facile removal. According to the elemental analysis conducted after precipitation and washing of the obtained microgels the sulfur content in the product was lower than 0.2 wt.%, suggesting very effective purification.

All examined samples of silsesquioxane microgels were synthesized in aqueous microemulsions based on dodecylbenzenesulfonic acid (DBA). Dynamic light scattering (DLS) allowed to evaluate the influence of DBA on the product dimensions directly after synthesis.

The basic characteristics of the obtained nanoparticles are summarized in Table 2.

The fleet ratio (F) – defined as surfactant-to-polymer (calculated for full monomer conversion) weight ratio is one of the basic parameters, describing microemulsion [23,24]. An increase in its value (up to the certain level) led to diameter reduction. However, undesired effects of diameter increase and higher product polydispersity were observed for higher DBA concentration (e.g. MG13 and MG15). Possible explanation could be different spatial distribution of surfactant particles (formation of other mesophases), but the experimental evidence is still lacking. Baumann et al. had observed similar phenomenon and assigned it to the decreasing microemulsion instability as well as interparticle agglomeration [23]. Though the recorded electron micrographs of MG13 and MG17 (see: Figs. 3 and 4, respectively) revealed more pronounced product

Table 2
Microgel nanoparticles – synthesis conditions and results

Microgel	F[a]	Particle diameter[b] [nm]	Bromine content[c] [wt.%]	Molecular weight × 10^6[d] [g/mol]
MG11	0.068	28.4	4.01	5.60
MG12	0.100	23.8	3.38	3.85
MG13	0.201	29.2	3.99	4.35
MG14	0.150	20.8	3.40	1.76
MG15	0.402	29.6	1.93	4.08
MG17	0.340[e]	15.6	3.06	0.96

[a] F – fleet ratio (surfactant/polymer weight ratio) [23,24].
[b] Determined by the dynamic light scattering (DLS).
[c] Determined by elemental analysis.
[d] Determined by the static light scattering (SLS).
[e] Initial amounts of reagents calculated as for the MG14, reduced amount of added monomer (details in the text).

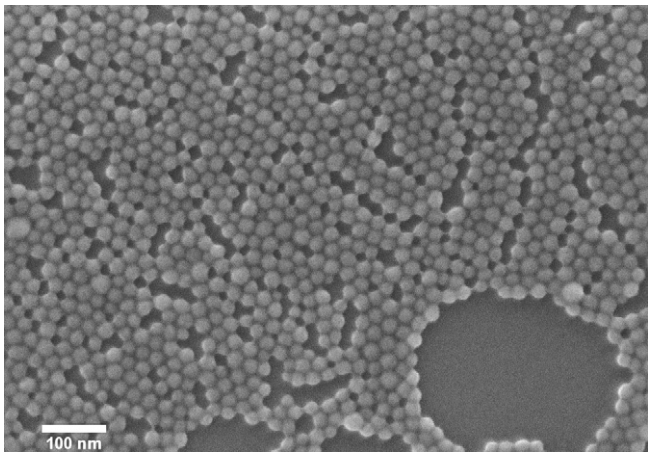

Fig. 3. SEM image of microgel MG13 nanoparticles (scale bar: 100 nm).

polydispersity, the particles preserved regular, spherical shape. If their assumption is right, the eventual agglomeration must occur at early stage of reaction. Upon reducing the monomer amount (at fixed DBA concentration – see: MG17) we were able to obtain smaller structures with diameters about 10 nm. The diameter reduction could be achieved at cost of increased polydispersity that should affect the results of the DLS and SAXS experiments (see Section 3.2). This issue will be treated in detail in further part of the article.

Scanning electron microscopy was used as the basic technique for preliminary assessment of the product quality. The recorded images (Figs. 3 and 4) revealed in most cases good control over particle shape – obtained microgels exhibited rather low dimensional polydispersity (e.g. 1.07 for MG12 as evaluated by the GPC – see Table 3). Even in case of the smallest nanoparticles MG17 (Fig. 4) regular shape seemed to be preserved.

3.2. Microgel characterization

Surface modification of the nanofiller particles was realized according to the procedure described by Savin et al. [18] and Pyun et al. [19]. As a consequence of an additional modification stage (in aqueous phase) higher degree of initiator immobilization could be achieved, reaching in case of the MG11 and MG13 almost 4 wt.%. This had severely influenced the activity of the macroinitiators for polymerization processes – as it will be shown further.

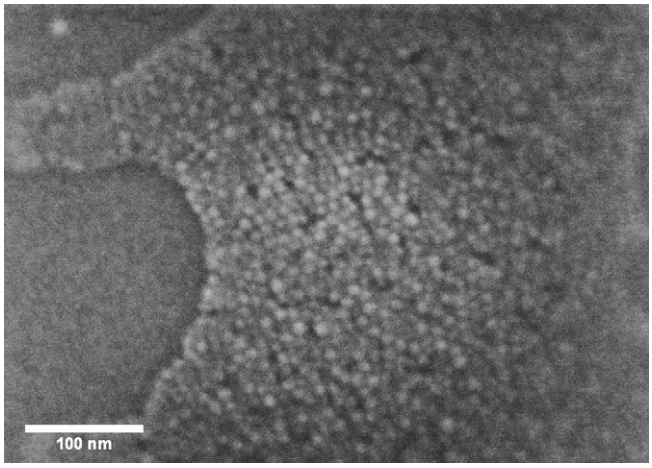

Fig. 4. SEM image of microgel MG17 nanoparticles (scale bar: 100 nm). Picture quality results from operating at the resolution limit and low object/support contrast.

Table 3
Results of the dynamic/static light scattering measurements of the microgel nanoparticles (dispersed in toluene)

Microgel	R_h[a] [nm]	R_g[a] [nm]	R_g/R_h	Molecular weight $\times 10^{-6}$[a] [g/mol]	Microgel density ρ_n[a] [g/cm^3]	PDI[b]	dn/dc[c] [cm^3/g]
MG11	14.2	16.9	1.19	5.60	0.775	1.14	−0.0481
MG12	11.9	11.9	1.00	3.85	0.906	1.07	−0.0447
MG13	14.6	16.1	1.10	4.35	0.554	1.11	−0.0463
MG14	10.4	12.9	1.24	1.76	0.620	1.10	−0.0523
MG15	15.7	23.3	1.48	4.08	0.499	1.42	−0.0487
MG17	7.8	21.5	2.76	0.96	0.799	1.21	−0.0403

[a] Determined with the DLS, the density was calculated for the swollen state.
[b] Polydispersity index (PDI), determined with GPC.
[c] Calculated from the dn/dc measurements.

The presence of the ATRP-initiating moieties was qualitatively confirmed via NMR experiments and elemental analysis. The ^{1}H NMR spectrum of the MG17 microgel in d_8-toluene is presented in Fig. 5.

All the NMR spectra collected for the reported microgels showed the presence of distinctly broadened signals. This effect was attributed to the reduced mobility of the groups constituting microgel network and is consistent with the observations reported elsewhere [30,32]. More noticeable smearing of the signals (as compared with T_8 polyhedral oligomers [32]) can be related to higher number of atoms and number of steric hindrances in the network. As a direct consequence not all expected peaks can be found in the spectra, some signals remain obscured. For assigning the peaks we referred to the analyses of similar systems published by other groups [22,32]. The broad peak observed at about 0.30 ppm, with a small shoulder at 0.54 ppm, is related to the protons of $-Si(CH_3)_3$ and $-Si(CH_3)_2-$ groups, respectively, whereas

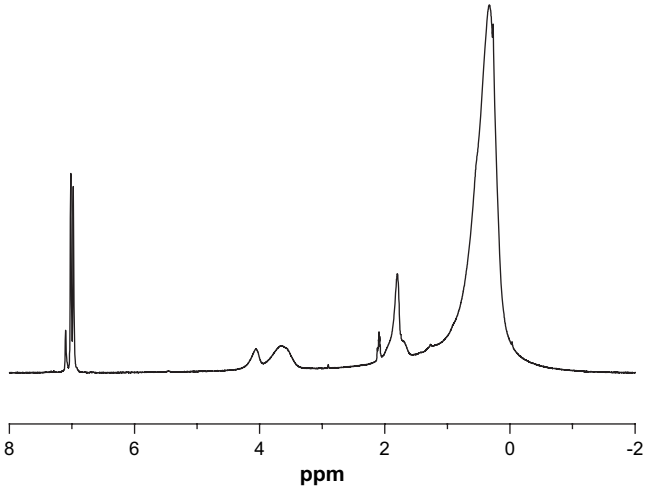

Fig. 5. ^{1}H NMR spectrum of the microgel MG17 (250 MHz; solvent: d_8-toluene).

the protons of $-CH_2-Si$ appear near to 0.85–0.9 ppm. In the range from about 1.6–1.9 ppm one can see the irregular group of overlapping signals from $-CH_2-$ (in β-position to Si atom) and $-CH_3$ protons of the initiator rest showing up at 1.60–1.80 and 1.90 ppm, respectively. The peak at about 3.60 could, in our opinion, orginate from unhydrolyzed $-OCH_3$ groups of the monomer, whereas the signal at 4.05 was assigned to the hydrogens of the $-CH_2-OCO-$ group. The latter signal provided a clear evidence for the immobilization of initiator. The solvent peaks (d_8-toluene) appear at around 2.10 and 7.00 ppm.

The ^{29}Si NMR measurements of the chosen microgels (deconvoluted spectra of the MG11 and MG14 – see Fig. 6) confirmed the successful immobilization of the initiator. The signal at about 8.8–8.9 ppm was attributed to the silicon atom coupled to the ATRP initiator rest [18]. Furthermore,

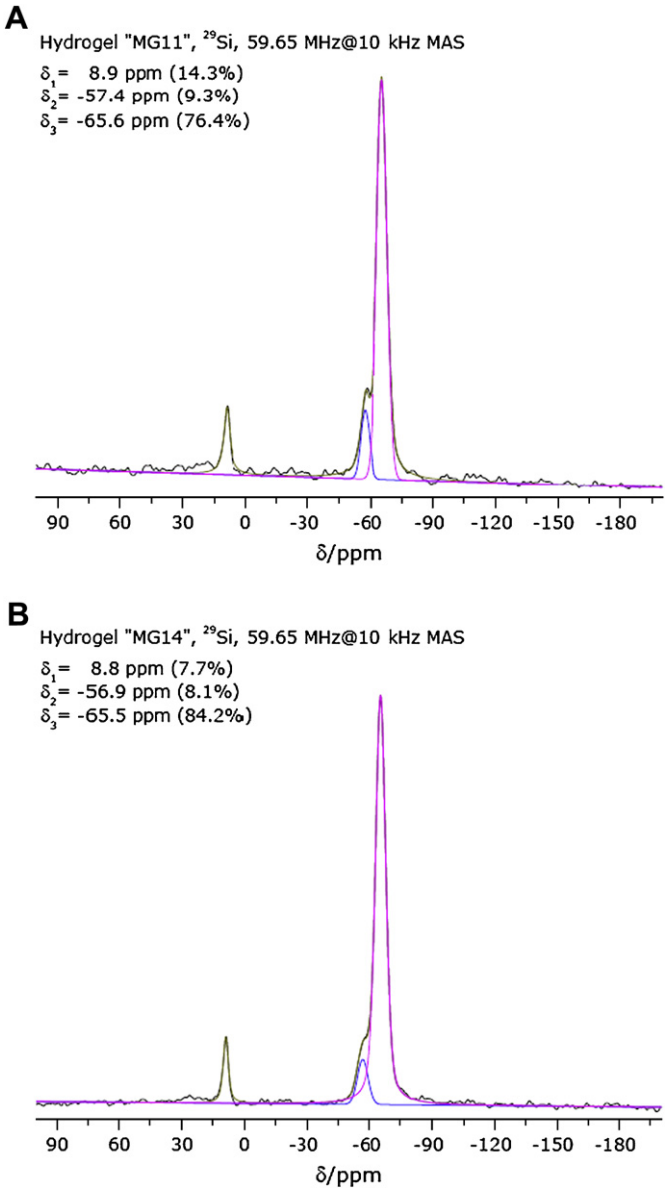

Fig. 6. The CPMAS ^{29}Si NMR spectra recorded for the microgels: MG11 (A) and MG14 (B).

we were able to characterize the internal structure of our gels. The main peak around −60 ppm comprised of resonances appearing at about −57 and −65.5 ppm, respectively, which were attributed to the silicon atoms having two (so-called T_2 resonance [30]) or three siloxane bonds (T_3). The obtained microgel network seems to be dense, but the peak intensity exhibits the reciprocal dependence with respect to the colloid diameter. For the smaller particles (MG14) the degree of silanol conversion (expressed by the T_2 intensity) is reduced when compared to the bigger structures (MG11), suggesting more effectively cross-linked structure. The bigger the particles, the more defects will occur during their formation leading finally to a rigid "gradient" network with more sterically excluded, non-converted alkoxy or silanol groups.

The elemental analysis at the University of Wroclaw enabled quantitative estimation of the attachment efficacy. By changing the molar ratio of ATRP–Et/Cl to 3MEtS (see Table 1) used, the amount of immobilized bromine became adjustable, leading to nanoparticles with various surface coverage. Due to the subsequent polymer grafting we were interested in obtaining high bromine content of about 3 wt.%. The modification could be carried out as early as at the first stage (in the aqueous phase) with the ATRP–Et initiator. However, reduced solubility of the compound in water remains the main obstacle and, in our opinion, may affect the modification process at this stage. After the microgel stabilization required to transfer the product quantitatively to the organic phase the modification had to be continued at elevated temperature using an excess of compound. Taking into consideration the data presented in Table 1 this was the crucial stage of reaction that allowed to control the amount of the immobilized initiator.

With respect to evaluation of grafting densities, the dimensional characterization of the nanoparticles became an issue of utmost importance. Static (SLS) and dynamic light scattering (DLS) measurements are the experimental techniques of common use in this relation that provide valuable information on physical properties as presented by Baumann et al. [23,24]. Results of the DLS/SLS measurements performed for our microgels are summarized in Table 3.

All synthesized microgel nanoparticles were characterized by relatively low (with respect to their dimensions) molecular weights (between $1.1–5.3 \times 10^6$ g/mol). This resulted in rather low density of the colloids (as calculated from the DLS), but similar effects had also been observed and described elsewhere [23,24]. In case of the MG15 and MG17 light scattering experiments were repeated. In both cases the obtained R_g values were surprisingly high, what in our opinion can result from higher – as detected by the GPC – product polydispersity.

The synthesized structures showed additionally an unexpected behavior of the R_g/R_h ratio (ζ). The ratios calculated for the systems (see Table 3) exceed the theoretical value of 0.775 characteristic for monodisperse hard spheres [23]. This suggests the obtained networks are rather loose and the solvent can penetrate particle interior quite easily. Such network morphology is the consequence of a polycondensation

process realized under acidic conditions. On the other hand, network swelling is expected to be rather limited as indicated by the ratio of R_g and M_w (in comparison with linear molecules in solution).

Possible explanation for the values of ζ may also be a certain dimensional polydispersity of nanoparticles. The bigger the particles, the more defects will occur leading finally to a rigid ''gradient'' network.

The experimental approach, limited only to the DLS/SLS experiments, turned out to be insufficient. The hydrodynamic radius depends strongly on polymer–solvent affinity and is rather not suitable for exact geometrical description of unswollen (''dry'') networks.

More reliable, statistical data can be collected, utilizing transmission electron microscopy (TEM) along with small-angle X-ray scattering (SAXS).

Two examples of TEM micrographs recorded for MG14 and MG15 are presented below (Figs. 7 and 8, respectively). Although the resulting products predominantly exhibited dimensional homogeneity, a quantitative analysis of the micrographs turned out to be complicated. The picture quality could not be severely improved at high magnifications, and formation of Fresnel rings was unavoidable (Fig. 8). In consequence, the relative error in diameter estimation could reach 10–15%. In case of the MG15 and MG17 the increased product polydispersity was observed, as mentioned earlier.

For almost all examined nanoparticles fairly well-resolved SAXS diffractograms were obtained. Peaks up to third order could be distinguished indicating rather narrow shape distribution. Only in case of the MG17 the resolution showed by the scattering profile is poor – probably as a result of more distinct polydispersity (as evidenced earlier). The examples of the scattering curves are depicted in Fig. 9.

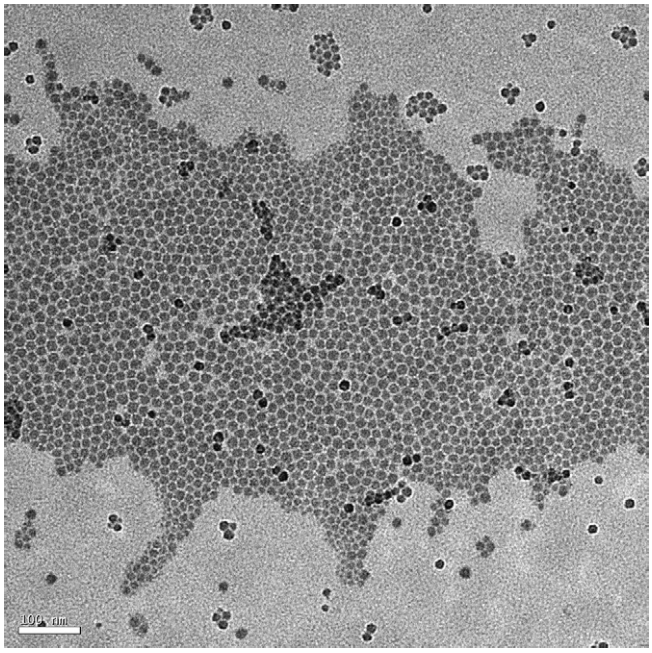

Fig. 7. TEM micrograph of the microgel MG14 (scale bar: 100 nm).

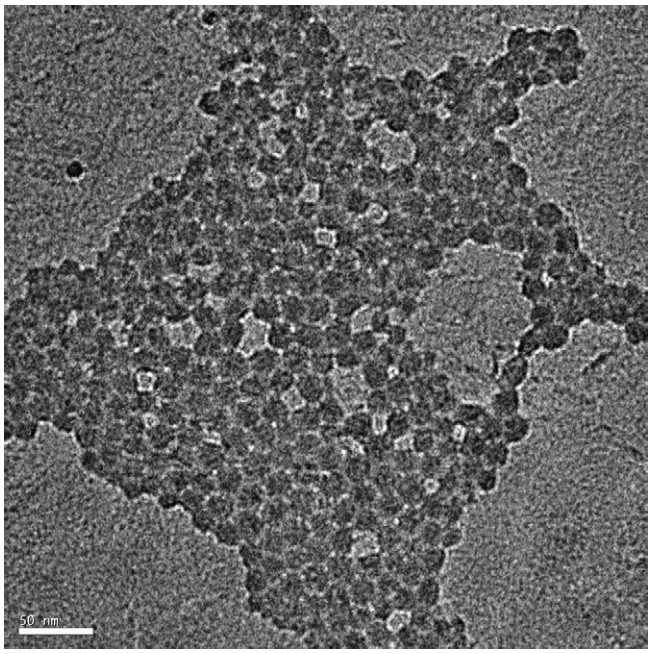

Fig. 8. TEM micrograph of the microgel MG15 (scale bar: 50 nm).

The obtained scattering profiles were complicated and had to be analyzed in terms of scattering and form factor. What could be anticipated is, the position of particular peaks in scattering patterns did not correspond to any regular spatial arrangement characteristic for highly organized materials (e.g. with FCC or BCC geometry). The first Bragg peak arising at low q values contained general information on the basic correlation length characterizing the system. It was particularly well pronounced in case of MG11 or MG14. The complete description of the structure required additionally the analysis of following peaks displaying the form factor. In conclusion the values of particle diameters were estimated [39].

The data, collected from the DLS, TEM and SAXS experiments, have been compared in Table 4.

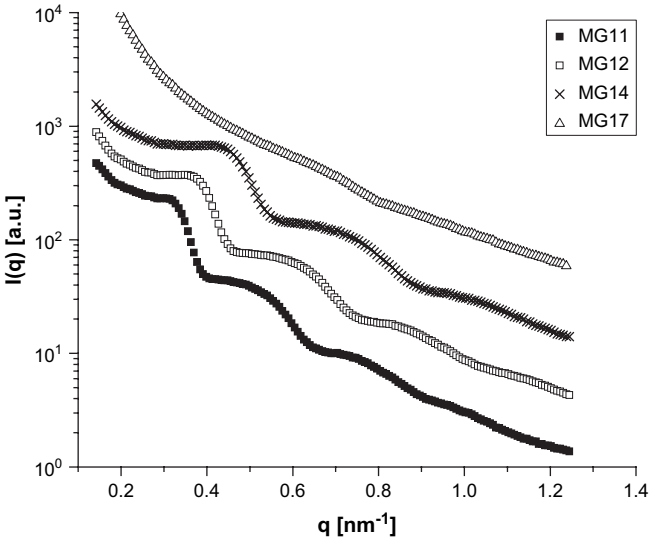

Fig. 9. Scattering profiles of the chosen microgel nanoparticles.

Table 4
Dimensions of the microgel nanoparticles estimated with the DLS, TEM and SAXS

Microgel	$\langle D_{DLS} \rangle = 2 \times R_h$ [a] [nm]	$\langle D_{TEM} \rangle$ [b] [nm]	$\langle D_{SAXS} \rangle$ [c] [nm]
MG11	28.4	22.8	19.7
MG12	23.8	19.1	16.8
MG13	29.2	22.2	19.2
MG14	20.8	17.5	14.1
MG15	29.6	19.4	15.3
MG17	15.6	11.0	10.6

[a] Determined with the DLS.
[b] Estimated from the TEM images.
[c] Estimated from the position of the first order Bragg peak.

As presented above, the DLS provides severely overestimated results in comparison with other techniques. The highest discrepancy of about 52% was observed in case of MG15. Naturally, grafting densities calculated on this basis would also be affected.

This overestimation may be a consequence of product polydispersity (scattering intensity scales as $\sim R^6$, R – being the particle radius, so the fraction of biggest particles in population scatters relatively stronger) and the presence of "shell" at particle's surface, consisting of solvent molecules with reduced mobility.

The inconsistency between TEM and SAXS results may arise from the problems emerging during evaluation of the micrographs (low contrast, Fresnel rings, limited number of the measured particles) rather than from the conditions of scattering experiments. The biggest deviation was observed for the MG14 and MG15 and reached about 20%, in other cases it did not exceed 15%.

3.3. ATRP polymerization

The silsesquioxane nanostructures, both polyhedral oligomers and amorphous colloids can be used as effective initiators of controlled polymerization processes after appropriate surface modification [33,40,41]. As early as in 2000 Pyun et al. succeeded in grafting vinyl monomers onto the surface of oligomeric silsesquioxanes [40] and silsesquioxane colloids [41] utilizing the copper-mediated ATRP and described the morphology of the hybrids by means of AFM [41]. Over following years, several research groups investigated various aspects of polymer grafting onto the silsesquioxane substrates [10,33]. Referring to above-mentioned works and results presented in papers [18,19] we were able to define the optimum conditions for surface-initiated ATRP processes.

The obtained microgels were characterized by higher bromine content, that should allow the preparation of structures with high grafting density. On the other hand, increased activity of such macroinitiator requires better control during the polymerization. Predominant product gelation (in consequence of recombination) can strongly reduce the reaction yield. The formation of ungrafted chains becomes an additional factor, affecting properties of the final product (especially when used as filler for modification of block copolymers).

We were interested in obtaining fairly high product yields with respect to the subsequent experiments on miscibility of grafted fillers within different systems (homopolymer, block copolymer). Hence, bigger amounts of macroinitiators were used (~1 g) and their average concentration reached even 3.5 wt.% with respect to the monomer.

The reaction conditions in particular experiments are summarized in Table 5.

First attempts to graft PS in a reaction carried out in bulk monomer and using only CuBr (catalyst) along with PMDTA (as ligand) were unsuccessful. At the catalyst/initiator ratio about 4 the reaction proceeded in an uncontrolled fashion, leading to considerable product gelation after about 1 h. Reduction in catalyst amount (to the catalyst/initiator ratio about 1) and addition of 10 mol.% of $CuBr_2$ (as described in [18,20]) as well as introduction of solvent (50 vol.%) led on contrary to an unacceptable suppression of the reaction rate (reaction times exceeded 100 h). Slow polymerization was observed also with bipyridine used as the ligand. Too long reaction times should be avoided because of the considerably higher probability of side-reactions.

Hence, we decided to modify the catalytic system by the addition of copper(II) bromide. Better polymerization control was obtained through a change in equilibrium between active and dormant species [42]. Good results – in terms of acceptable product yield and reaction rates – were achieved, when the amount of CuBr reached almost 2-fold concentration of the initiator used and the content of $CuBr_2$ was about 50 mol.%. The reaction times varied between 15 and 72 h. The synthesized polymer was characterized by M_w ranging from about 8500 to almost 30 000 g/mol and narrow polydispersity (polydispersity index, PDI – typically 1.10). As expected, the determining factor was the amount of Cu(II) used – its reduction to 40 mol.% caused significant acceleration of the process (stopped after 16 h). The low values of polydispersity (in comparison to the systems based on bipyridine [18]) are certainly related to higher complexing efficiency, typical for multidentate amines (PMDTA, HMTETA).

It was necessary to interrupt polymerizations at relatively low conversion to suppress the risk of interparticle coupling by radical recombination. In two cases (P11PS and P20PS) the conversion reached the level, when partial gelation of the product occurred. Generally, our results correlated well with the observation of Savin and coworkers, setting the upper limit of monomer conversion about 15 wt.% [18].

The formation of free polymer was another issue, particularly important with respect to the filler properties. Originally observed during the ATRP of styrene by von Werne and Savin, it was suggested to occur in diluted (i.e. characterized by a high monomer-to-initiator ratio reaching 1000:1) [18,20]. Referring to our experiments, we would assume the polymerization time to be the main factor. The mentioned concentration ratio in our experiments was ranging from 423:1 to 606:1, but the formation of ungrafted chains was clearly observed in all cases (as presented in Table 1). The lowest amount of free polymer was observed in case of a relatively

Table 5
ATRP of styrene initiated with functionalized silsesquioxane microgels- conditions and results[a]

Product (core-shell structure)	Microgel	Catalyst/initiator molar ratio	$CuBr_2$ [mol.%]	Amount of free PS[b] [wt.%]	Monomer conversion[c] [wt.%]	$M_{w,\ hairs}$[d] [g/mol]	PDI[d]
P09PS	MG11	0.76	54.24	19.65	2.96	8250	1.11
P10PS	MG12	2.11	42.26	20.43	7.18	21 880	1.20
P11PS		2.14	42.43	20.88	25.20[e]	29 530	1.11
P12PS		1.78	45.45	31.15	13.41	24 000	1.10
P13PS		1.71	44.96	21.57	10.66	16 950	1.10
P14PS	MG14	1.70	47.61	12.21	19.43	21 850	1.07
P17PS		1.54	47.07	4.23	11.35	13 250	1.09
P18PS	MG17	1.73	47.07	10.00	12.98	11 750	1.06
P20PS		1.55	39.80	10.91	30.05[e]	17 240	1.09

[a] All reactions were carried out in solution (solvent – toluene, solvent volume fraction ~50 vol.%, ligand – PMDTA) and at 90 °C.
[b] Determined with the GPC.
[c] Estimated gravimetrically.
[d] Determined with the GPC after cleaving reaction with HF.
[e] Partial gelation of the product occured.

short process (P14PS – 22 h, P17PS – 16 h), the highest was recorded for P12PS (36 h; reaction was stopped and initiated again by heating). To prove our assumption, we decided to run an additional polymerization (not specified in the table) – the reaction was conducted with an reduced charge (40% of the average reagent amount), at lower temperature (85 °C) and with the amount of $CuBr_2$ increased to 65 mol.%. After 72 h the M_w of the grafts reached nearly 9000 g/mol, but the free polymer content simultaneously exceeded 22 wt.%.

The example image of the core-shell structure is presented in Fig. 10.

3.4. Characterization of the core-shell structures

During the investigation of polymer-grafted nanoparticles we tried to find the answers for two major questions:

(a) What is the exact amount of grafted polystyrene?
(b) What are the values of parameters describing the distribution of tethered chains on the filler surface?

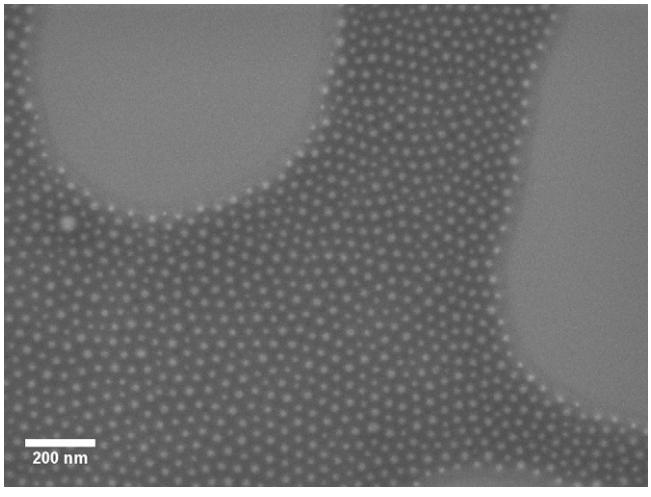

Fig. 10. SEM image of the core-shell structure P11PS (core: microgel MG12, shell: PS 29530 g/mol, scale bar: 200 nm).

The amount of grafted PS was evaluated using thermogravimetry (TGA) and refractive index increment (d*n*/d*c*) analysis, as suggested elsewhere [10]. The results of both experiments are summarized in Table 6.

The obtained values allowed to calculate grafting densities, by making an assumption defining the dimensions of microgel particles. The diameters derived from the SAXS curves were chosen as relevant measure of unswollen networks. The detailed information on mathematical formalism is presented in the attached Appendix.

Taken into consideration bromine content (elemental analysis) the initiating efficiency (ratio of the number of grafted PS chains to the total number of immobilized initiating moieties) was evaluated.

The results of TGA allowed for the presence of organic groups on neat nanoparticles, the values from the d*n*/d*c* measurements were slightly higher in almost all cases. The differences varied form 1.5% to about 6.5%.

The analysis of initiator efficiency provided valuable information. However, in this case one had to take into account the specificity of utilized microgels. Quite loose network resulted probably in a significant number of sterically-hindered (e.g. closed in pores) initiating moieties, thus lowering the initiator efficiency. In general, bigger particles should contain

Table 6
Core-shell structures- amount of grafted PS and grafting densities

Product	Microgel	Polymer amount [wt.%]		Grafting density [nm^{-2}]		Initiator efficiency[a] [%]
		TGA	d*n*/d*c*	TGA	d*n*/d*c*	
P09PS	MG11	47.70	50.79	0.31	0.35	18.1
P10PS	MG12	58.12	59.50	0.17	0.18	11.9
P11PS		77.33	76.50	0.31	0.29	20.4
P12PS		72.81	75.86	0.26	0.30	19.1
P13PS		65.16	66.17	0.29	0.30	20.2
P14PS	MG14	75.83	83.98	0.24	0.39	38.7
P17PS		71.96	78.49	0.34	0.48	51.3
P18PS	MG17	71.53	73.50	0.49	0.60	54.4
P20PS		80.59	83.22	0.54	0.65	59.6

[a] Average value from the TGA and d*n*/d*c* experiments.

larger number of them (less advantageous surface-to-volume ratio). This assumption was confirmed for the examined systems (see Table 6) – the smaller the particles, the higher the initiator efficiency. In case of P10PS, the slightly reduced value along with higher PS polydispersity should be explained with perturbed reaction control probably at the early stage. In consequence, higher fraction of the surface could be excluded and blocked by polymer chains growing too fast.

Differential scanning calorimetry (DSC) and X-ray scattering (SAXS) were used in order to answer the question that concerned the values of parameters describing the surface distribution of tethered chains. In this sense, we were particularly interested in unique behavior of polymer chains resulting from dense grafting.

The chains attached to the surface constitute a polymer brush, when the dense packing forces them to stretch away (at the cost of the reduction in conformational entropy). Such a system will exhibit interesting physical properties – among others, this unique ordering of macromolecules affects their miscibility with polymer matrices [10].

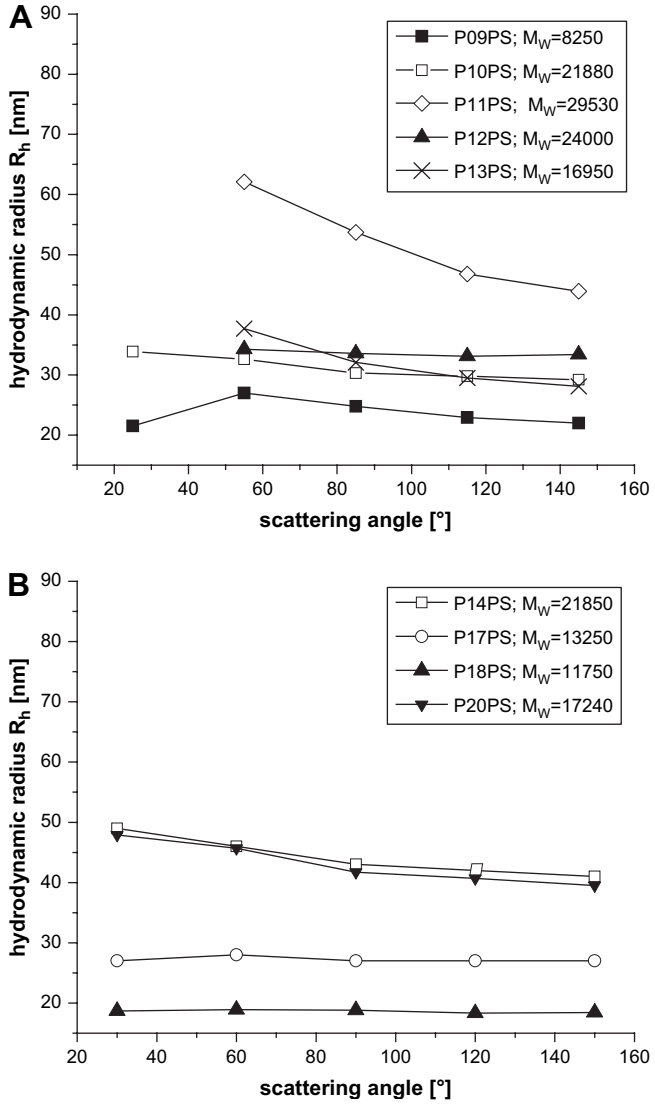

Fig. 11. Results of the DLS experiments for the core-shell structures: (A) based on the microgels MG11 and MG12; (B) based on the microgels MG14 and MG17. The lines are added to guide the eye.

To confirm the grafting of polymer chains, the DLS measurements were performed for the toluene dispersions of core-shell structures. The technique is characterized by high sensitivity towards the presence of agglomerated structures. The results of examination are depicted in Fig. 11A and B.

Generally, we did not observe strong angular dependencies of hydrodynamic radius R_h for processes stopped at conversion lower than 14 wt.% (relatively low M_w of PS "hairs", except of P12PS). This allowed us to conclude that there was no severe interparticle coupling in consequence of radical recombination. On the other hand the angular dependencies of Rh observed in case of P13PS, P14PS, P20PS and, particularly, P11PS, suggest the presence of some agglomerated structures. Lower amount of copper(II) bromide, moderating the reaction rate, and higher conversion (except of P13PS) are probable explanations for that phenomenon.

The investigation of a similar system PS-*g*-SiO_2 nanoparticles provided evidence, that the T_g of polymer is a very sensitive probe the state of chain deformation. Hence, the DSC calorimetry has become a valuable tool to analyze core-shell structures [18]. The influence of chain stretching usually observed in case of grafted polymer brushes can be highlighted by a simple comparison with the T_g of chains cleaved from the surface.

The results recorded for PS-*g*-μgels (used as fillers in further experiments) are listed in Table 7. We were able to complement the observations of Savin and coworkers with additional information [18]. Analyzing the results, one must keep in mind, how complicated systems were investigated. In our opinion following parameters must be taken into account the M_w of the PS "hairs", their grafting density, amount of free polymer and the surface curvature (defined as the reciprocity of particle radius).

The obtained results seem to correlate well with those presented elsewhere [18]. We stated the reciprocal relation between the M_w and the change in T_g, either. In case of four

Table 7
Comparison of T_g for cleaved and grafted polystyrene

Product	T_g of the cleaved PS[a] [°C]	T_g of the grafted PS[a] [°C]	ΔT_g	M_w of the grafted PS[b] [g/mol]	Grafting density[c] [nm^{-1}]
P09PS	85.3	97.2	11.9	8250	0.33
P10PS	96.9	98.8	1.9	21 880	0.17
P11PS	98.6	100.8	2.2	29 530	0.30
P12PS	98.3	102.5	4.3	24 000	0.28
P13PS	94.3	100.6	6.3	16 950	0.30
P14PS	97.7	103.7	6.0	21 850	0.31
P17PS	94.2	101.5	7.2	13 250	0.41
P18PS	91.7	98.7	7.0	11 750	0.54
P20PS	94.8	101.4	6.6	17 240	0.59

[a] Estimated from the DSC experiments, heating rate 10 K/min.
[b] Determined with the GPC.
[c] Average value calculated from the TGA and d*n*/d*c* experiments, particle area was estimated from TEM images.

systems exhibiting almost equal grafting density of about 0.3 molecule/nm^2 (a simplifying assumption for the systems P09PS and P11PS–P13PS), similar amount of free polymer (about 20 wt.%) and nearly uniform surface curvature (0.088 and 0.105 [nm^{-1}] for the core of MG11 and MG12, respectively) the highest value of ΔT_g has been observed for the shortest chains. This behavior can be easily explained taking into consideration the presence of a gradient in the density of monomer units perpendicular to the curved surface. The fairly short molecules (P09PS) are subjected to deformation on a significant length-scale, in case of the longest investigated chains (P11PS) the stretching of an initial fragment of the molecule cannot influence its overall behavior. Additional factor arises with the extent of surface curvature – the more planar the substrate, the longer the deformed part of the chain should be. This is the probable explanation for significant value of the interval ΔT_g in case of the product P09PS. Naturally, the presence of free, ungrafted chains should also be taken into consideration – at least for the upper ''layer'' of the brush, where the reduced steric hindrance allows them to penetrate the polymer shell. Nevertheless, additional experiments with purified (e.g. by ultrafiltration) core-shell fillers are required in order to clarify this.

Keeping in mind all the needed simplifying assumptions stated above (concerning grafting density, free polymer content and filler geometry), we additionally made an attempt to estimate the limiting value of the M_w, in which the difference between tethered and free PS chains should vanish. The dependence between M_w and ΔT_g for the mentioned systems (P09PS, P11PS–P13PS) is depicted in Fig. 12.

For the analyzed conditions we obtained an almost linear relationship of both parameters. From the intersection the limiting value of approximately 35 kg/mol was estimated.

Referring to other obtained structures, in case of the P10PS the previous assumption of low grafting density was additionally confirmed by a fairly low ΔT_g of about 1.9 °C.

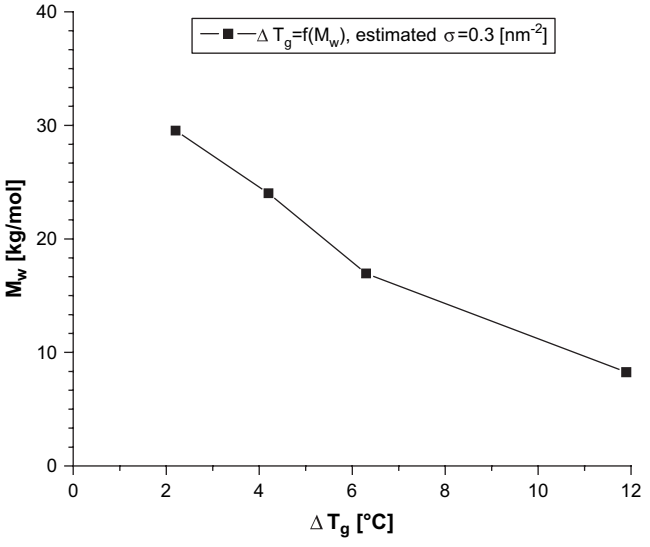

Fig. 12. ΔT_g as a function of M_w (assumed value of the grafting density: 0.3 chain/nm^2). The line is added to guide the eye.

The analysis of the systems based on smaller particles – the products P14PS, P17PS, P18PS and P20PS based on the cores of MG14 and MG17 – brought some intriguing results, either. Relatively high values of the interval ΔT_g emphasize the influence of higher grafting densities. Due to the lowest amount of ungrafted PS, the product P17PS is especially interesting, because the measured T_g approximates the value expected for pure core-shell system. On the other hand, relatively lower values of T_g in case of the products P18PS and P20PS could undoubtedly be related to higher surface curvature, reducing the length of the deformed fragment of the chain.

4. Concluding remarks

Silsesquioxane microgel nanoparticles exhibiting well-defined shape and diameters lower than 30 nm were synthesized in microemulsion, and surface modified with an ATRP initiator. The amount of bromine determined by elemental analysis was relatively high (over 3 wt.%, on average), resulting in correspondingly high activity of these macroinitiators in polymerization processes. In order to obtain reliable data on grafting density, particle dimensions were extensively investigated with SAXS, TEM and DLS.

Organic–inorganic structures consisting of a silsesquioxane core with a grafted polystyrene shell were successfully prepared according to the ATRP technique. The best results were achieved using the catalytic system with a medium excess of copper(I) bromide (towards initial concentration of initiator) and considerably high content of copper(II) bromide (50 mol.% on average). We were not interested in a detailed process characterization (kinetic investigation).

According to our observation, the formation of ungrafted polymer in the course of reaction is related mainly to polymerization time, at least for the examined values of monomer-to-initiator ratio. The presence of the free chains creates additional complications, when the core-shell structures are used as fillers. During our experiments we were able to reduce the amount of non-grafted PS to about 10–20 wt.%.

The obtained core-shell structures were characterized in detail using light scattering (SLS, DLS), TGA, electron microscopy (TEM, SEM) and SAXS. The results suggest that PS chains are relatively densely grafted and stretched. The grafting density and M_w of the attached chains is expected to affect the interactions of the core-shell fillers and the modified polymer matrix, thereby defining the nanocomposite performance. We observed reciprocal dependencies between grafting density and initiator efficiency, and surface curvature (particle dimensions), as expected. For bigger particles (MG11 and MG12 with diameters of about 23 and 20 nm, respectively) grafting density of about 0.3 chain/nm^2 was found by average initiator efficiency about 20%, whereas for the smallest particles used (MG17) both parameters reached the values of nearly 0.6 chain/nm^2 and 60%, respectively. In case of bigger nanoparticles, the number of sterically excluded initiator groups is believed to be the main reason.

Acknowledgements

The authors would like to express deep gratitude to following persons:

- Prof. Dr. S. Förster (University of Hamburg) for inspiring discussions concerning evaluation of SAXS data;
- Prof. Dr. W. Steffen (MPIP, Mainz) for valuable suggestions concerning light scattering experiments;
- Dr. G. Brunklaus (MPIP, Mainz) for conducting the ^{29}Si NMR measurements and data evaluation;
- Mrs. Ch. Hermann, Mrs. M. Müller and Dr. I. Lieberwirth (MPIP, Mainz) for conducting thermal experiments, scanning and transmission microscopic investigation (SEM), respectively;
- Mr. G. Kircher (MPIP, Mainz) for preparation and purification of ATRP–Cl initiator used in experiments;
- Mrs. S. Seywald and U. Heinz (MPIP, Mainz) for the GPC analyses.

The financial support of the Marie-Curie Program is gratefully acknowledged (grant: MEST-CT-2004-513924).

Appendix

For the calculation of the parameters described in text we made use of mathematical formalism proposed elsewhere [10,24].

1. The density of the microgel network (in dispersion) can be calculated using formula (1):

$$\rho_{\mathrm{netw}} = \frac{\langle M_{\mathrm{w\ particle}} \rangle}{\langle V_{\mathrm{particle}} \rangle \times N_{\mathrm{A}}}, \tag{1}$$

the values of the $\langle M_{\mathrm{w}} \rangle$ of the microgel and $\langle R_{\mathrm{h}} \rangle$ (mean hydrodynamic radius) of the spherical particle are measured during the DLS experiment. The volume can be calculated from the relation $4\pi(R_{\mathrm{h}})^3/3$.

2. Other parameters were estimated utilizing following formulae [10,24].

   (a) The initiator density [1/nm^2]:

$$\rho_{\mathrm{in}} = \frac{\text{moles Br}}{\text{moles microgel} \times \text{particle surface}},$$

the amount of bromine is estimated according to elemental analysis. Particle surface is calculated according to the relation $4\pi R^2$, where R denotes particle radius measured with the chosen method (DLS, SAXS or TEM).

   (b) The fraction of PS in dn/dc measurements [wt.%]

$$\mathrm{PS}_{\mathrm{d}n/\mathrm{d}c} = \left(\frac{(\mathrm{d}n/\mathrm{d}c)_{\mathrm{PS}\text{-}g\text{-}\mu\mathrm{gel}} - (\mathrm{d}n/\mathrm{d}c)_{\mu\mathrm{gel}}}{(\mathrm{d}n/\mathrm{d}c)_{\mathrm{PS}} - (\mathrm{d}n/\mathrm{d}c)_{\mu\mathrm{gel}}} \right) \times 100\%,$$

refractive index increment for all substances must be measured by separate experiments.

   (c) The fraction of PS in TGA experiments (the results were additionally corrected for the mass loss of the microgel) [wt.%]:

$$PS_{\mathrm{TGA}} = \left(1 - \frac{X_{\mathrm{PS}\text{-}g\text{-}\mu\mathrm{gel}}}{X_{\mu\mathrm{gel}}} \right) \times 100\%,$$

where: $X_{\mathrm{PS}\text{-}g\text{-}\mu\mathrm{gel}}$ and $X_{\mu\mathrm{gel}}$ denote the amounts of residuals left after TGA of the core-shell structure and corresponding, bare microgel [both expressed in wt.%], respectively.

   (d) The grafting density of polystyrene chains [1/nm^2]:

$$\rho_{\mathrm{PS}} = \frac{\text{moles PS}}{\text{moles microgel} \times \text{particle surface}},$$

the molar amount of polystyrene can be calculated, provided the molecular weight and amount (mass) of the polymer in the sample are known.

References

[1] Messersmith P, Giannelis EP. Journal of Polymer Science A 1995;33:1047–57.
[2] Shi H, Lan T, Pinnavaia TJ. Chemistry of Materials 1996;8:1584–7.
[3] Ishifuji M, Mitsuishi M, Miyashita T. Applied Physics Letters 2006;89:011903.
[4] Li Y, Cai W, Cao B, Duan G, Sun F. Polymer 2005;46:12033–6.
[5] Oey C, Djurisic AB, Kwong CY, Cheung CH, Chan WK, Nunzi JM, et al. Thin Solid Films 2005;492:253–8.
[6] Cheng YJ, Gutmann JS. Journal of the American Chemical Society 2006;128:4658–74.
[7] Beek WJE, Wlenk MM, Janssen RAJ. Advanced Functional Materials 2006;16:1112–6.
[8] Zhang H, Cui Z, Wang Y, Zhang K, Ji X, Lü C, et al. Advanced Materials 2003;15:777–80.
[9] Wang ZM, Chung TC, Gilman JW, Manias E. Journal of Polymer Science B 2003;41:3173–87.
[10] Lindenblatt G, Schärtl W, Pakula T, Schmidt M. Macromolecules 2000;33:9340–7.
[11] de Gennes P. Macromolecules 1980;13:1069–75.
[12] Shull KR. Journal of Chemical Physics 1991;94(8):5723–38.
[13] Shull KR. Macromolecules 1996;29:2659–66.
[14] Borukhov I, Leibler L. Macromolecules 2002;35:5171–82.
[15] Maas JH, Fleer GJ, Leermakers FAM, Cohen Stuart MA. Langmuir 2002;18:8871–80.
[16] Corbierre M, Cameron N, Sutton M, Mochrie SGJ, Lurio LB, Rühm A, et al. Journal of the American Chemical Society 2001;123:10411–2.
[17] Corbierre M, Cameron N, Sutton M, Laaziri K, Lennox RB. Langmuir 2005;21:6063–72.
[18] Savin D, Pyun J, Patterson GD, Kowalewski T, Matyjaszewski K. Journal of Polymer Science B 2002;40:2667–76.
[19] Pyun J, Jia S, Kowalewski T, Patterson GD, Matyjaszewski K. Macromolecules 2003;36:5094–104.
[20] von Werne T, Patten TE. Journal of the American Chemical Society 2001;132:7497–505.
[21] Holzinger D, Liz-Marzan LM, Kickelbick G. Journal of Nanoscience and Nanotechnology 2006;6:445–52.
[22] Ramakrishnan A, Dhamodharan R, Rühe J. Macromolecular Rapid Communications 2002;23:612–6.
[23] Baumann F, Schmidt M, Deubzer B, Geck M, Dauth J. Macromolecules 1994;27:6102–6.
[24] Baumann F, Deubzer B, Geck M, Dauth J, Schmidt M. Macromolecules 1997;30:7568.
[25] Emmerich O, Hugenberg N, Schmidt M, Sheiko SS, Baumann F, Deubzer B, et al. Advanced Materials 1999;11:1299–303.

[26] Graf C, Schärtl W, Fischer K, Hugenberg N, Schmidt M. Langmuir 1999;15:6170–80.
[27] Jungmann N, Schmidt M, Maskos M. Macromolecules 2001;34: 8347–53.
[28] Jungmann N, Schmidt M, Maskos M, Weis J, Ebenhoch J. Macromolecules 2002;35:6851–7.
[29] Bumbu G, Kircher G, Wolkenhauer M, Berger R, Gutmann JS. Macromolecular Chemistry and Physics 2004;205:1713–20.
[30] Loy D, Rahimian K. Building hybrid organic–inorganic materials using silsesquioxanes. In: Nalwa HS, editor. Handbook of organic–inorganic hybrid materials and nanocomposites, vol. 1. American Sci Publ; 2003. p. 81–141.
[31] Pan G, James ME, Schaefer DW. Journal of Polymer Science B 2003;41: 3314–23.
[32] Mori H, Lanzendörfer MG, Müller AEH, Klee JE. Macromolecules 2004;37:5228–38.
[33] Mutukrishnan S, Plamper F, Mori H, Müller AEH. Macromolecules 2005;38:10631–42.
[34] Ma C, Taniguchi I, Miyamoto M, Kimura Y. Polymer Journal (Tokyo) 2003;35:270–5.
[35] Bogush GH, Tracy MA, Zukoski CF. Journal of Non-Crystalline Solids 1988;104:95–106.
[36] Arrigada FJ, Osseo-Asare K. Journal of Colloid and Interface Science 1995;170:8–17.
[37] Chang CL, Fogler HS. Langmuir 1997;13:3295–307.
[38] Buining PA, Liz-Marzan LM, Philipse AP. Journal of Colloid and Interface Science 1996;179:318–21.
[39] Jakuczek L, Gutmann JS. Polymer, submitted for publication.
[40] Pyun J, Matyjaszewski K. Macromolecules 2000;33:217–20.
[41] Pyun J, Matyjaszewski K, Kowalewski T, Savin D, Patterson G, Kickelbick G, et al. Journal of the American Chemical Society 2001;123:9445.
[42] Matyjaszewski K, Xia J. Chemical Reviews 2001;101:2921–90.